Bull. Natl. Mus. Nat. Sci., Ser. C, 37, pp. 17–27, December 22, 2011

SHRIMP U–Pb Zircon Geochronology of the Orthogneiss and Paragneiss in the Eastern Central Range, Taiwan

Yukiyasu Tsutsumi[1]*, Kazumi Yokoyama[1], Jason Jiun-San Shen[2], Kenji Horie[3], Kentaro Terada[4], Hiroshi Hidaka[4] and Chun-Sun Lee[5]

[1] Department of Geology and Paleontology, National Museum of Nature and Science, 4–1–1 Amakubo, Tsukuba, Ibaraki 305–0005, Japan
*Author for correspondence: ytsutsu@kahaku.go.jp
[2] Institute of Earth Science, Academia Sinica, Taipei, Taiwan, R.O.C.
[3] National Institute of Polar Research, 10–3 Midori-cho, Tachikawa 190–8518, Japan
[4] Department of Earth and Planetary Sciences, Graduate School of Science, Hiroshima University, Higashi-Hiroshima, Hiroshima 739–8526, Japan
[5] Department of Earth Sciences, National Taiwan Normal University, Taipei, Taiwan, R.O.C.

Abstract Radiometric ages of zircons from three gneiss samples in the Tailuko Belt from Eastern Central Range, Taiwan, were obtained from $^{238}U/^{206}Pb$ ratios using a Sensitive High Resolution Ion MicroProbe (SHRIMP II). The zircons in the orthogneiss sample YG29J1 from Nanao show one age cluster, and their weighted average is 82.2±1.3 Ma. Zircons in the paragneiss samples TW64 and TW65 from Chipan show rim ages concentrated at 83.2±1.2 Ma, which indicates a metamorphic age consistent with the age of the orthogneiss YG29J1. On the other hand, the core ages of the paragneiss range mainly from 90 to 220 Ma with a small number of older cores ranging from 1800–2000 Ma. Anhedral to subhedral structures of the zircon core, the coarse-grained nature, and the age variation show that their protoliths are sandstone, i.e. Cretaceous sandstones. The youngest zircon core, with an age of 95 Ma, marks the older limit of deposition age for the protoliths. Hence, it is reasonable to conclude that the rocks underwent extensive magmatism and metamorphism 82–83 Ma after deposition.

Key words : Taiwan, gneiss, deposition age, metamorphic age, zircon, U–Pb age

Introduction

The Taiwan Island is composed of six geological provinces: the Coastal Plane, Western Foothills, Western Central Range, Eastern Central Range, Longitudal Valley, and Coastal Range, from west to east (Fig. 1). The provinces form long narrow belts roughly parallel to the long axis of the island. It is thought that Taiwan was formed by the collision of an island arc (now the Coastal Range) with the margin of the continental plate, where a convergent plate boundary between the Eurasian and the Philippine Sea plates was located. Geologic belts on Taiwan Island have a propensity to be younger progressively westward from the Eastern Central Range to the west coast, not counting the Longitudal Valley and Coastal Range. The Eastern Central Range (Tananao Complex) is located on the western side of the Longitudinal Valley, and consists of many varieties of Pre-Tertiary rocks—either sedimentary, igneous, or metamorphic in origin—which underwent post multimetamorphism and were inevitably highly complicated geologic structures. The gneisses have especially been considered to be part of older rocks in the Eastern Central Range.

In order to clarify the depositional age of the gneisses on the Taiwan Island, we analyzed zircons from both orthogneiss and paragneiss samples and measured U–Pb ages using SHRIMP II equipment installed at Hiroshima University,

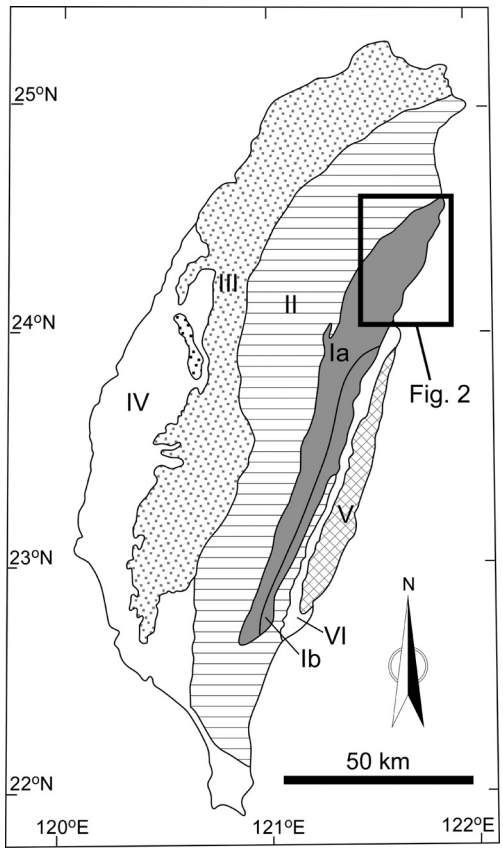

Fig. 1. Geological division of Taiwan. I: Eastern Central Range (Ia: Tailuko Belt; Ib: Yuli Belt); II: Western Central Range; III: Western foothills; IV: Coastal plain; V: Coastal Range; IV: Longitudal Valley.

Japan. The closure temperature of the U–Pb system for zircon is higher than 900°C, and the system usually remains closed under low- to medium-grade metamorphism (Lee *et al.*, 1997; Sano *et al.*, 1999; Cherniak and Watson, 2000). So the ages of zircons in these rocks have not been significantly disturbed during metamorphism and therefore provide information on the ages of the gneiss protoliths.

Geological Settings

The Eastern Central Range is subdivided into two belts: the Tailuko and the Yuli belts. The Tailuko Belt is in the western part of the Eastern Central Range which is the metamorphic complex on the Taiwan Island. The belt consists mainly of pelitic schist, gneiss, migmatite, metamorphosed limestone, greenschist, siliceous schist, and amphibolite. Although most of the rocks in the belt indicate low-grade greenschist facies, intermediate-grade metamorphic amphibolite facies or even higher grade facies occur in the northern part of the belt. This is illustrated by the existence of amphibolite, paragneiss, granitic intrusion, migmatite, and by the occurrence of sillimanite in parts of the area. On the other hand, the Yuli Belt is composed mainly of a monotonous series of pelitic schist with a minor amount of green schist. (Ho, 1986b)

The Tailuko Belt is the oldest geologic province on Taiwan Island. Except for model ages, 250±20 Ma (Sr isotopic stratigraphy; Jahn *et al.*, 1984) for marble is the oldest numerical age for the belt. Fusulinids assemblages also demonstrate that parent sediment of the marble was deposited in the Permian (Lee, 1984). The oldest metapelite age is older than 175 Ma, which was determined by finding the dinoflagellate fossile *Eyachia* (?) (175–200 Ma; Chen, 1989). On the other hand, marble from a deep drilling core beneath the Coastal Plane indicate**s** 242±22 Ma (whole-rock Pb–Pb isochron; Jahn *et al.*, 1992). So, for the Eastern Central Range, it is thought that old basement rocks at deeper depths were curled or extruded up by the force of the Luzon arc (now Coastal Range) collision (*e.g.* Ho, 1986a; Yen and Yeh, 1990). There are four stages of tectono-thermal events in Taiwan based on various dating methods: 1) the early Mesozoic (200 to 175 Ma), 2) the late Mesozoic (97 to 77 Ma), 3) the Cenozoic (37 to 8 Ma), and 4) the ongoing (3 Ma to present) event (Lan *et al.*, 1996).

Samples and Analytical Methods

In the Tailuko Belt, there are six prominent gneiss bodies which were named by Yen (1954): namely the Kiyoku, Yuantoushan, Fanpaochienshan, Tachoshui, Kanagan, and Takkiri. Three

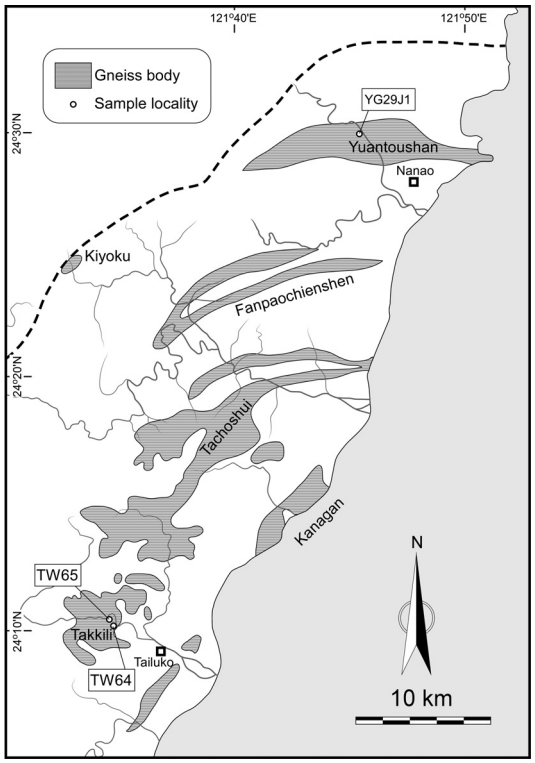

Fig. 2. Distribution map of gneiss bodies in northern part of the Tailuko Belt.

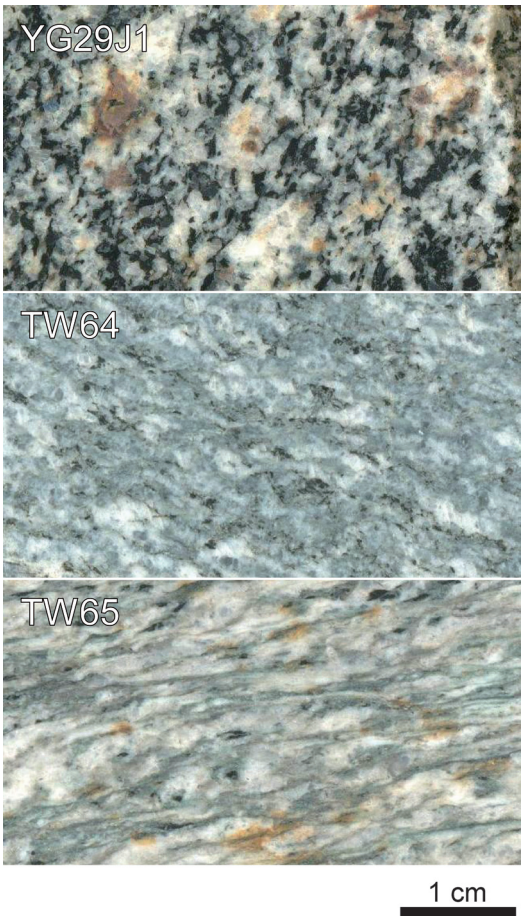

Fig. 3. Photographs of slabs of the samples; a) YG29J1, b) TW64 and c) TW65.

gneiss samples, YG29J1, TW64, and TW65 were collected from the northern part of the Tailuko Belt (Fig. 2). YG29J1 is from the Yuantoushan gneiss body near Nanao. TW64 and TW65 are from a small gneiss body in the Takkiri which is also called the Chipan Gneiss (*e.g.* Chen, 1963). YG29J1 is scarcely deformed granodioritic orthogneiss (Fig. 3a) that is found to be equigranular under magnification by an optical microscope. YG29J1 is composed mainly of quartz, plagioclase, biotite, and K-feldspar (Fig. 4a), while garnet, titanite, and hornblende are subordinate in quantity. As secondary minerals, chlorite, muscovite, and epidote occur replacing coarse-grained biotite and feldspars. TW64 and TW65 collected from the Chipan gneiss are found to be sheared gneisses by macro and microscopic observations (Fig. 3b and c; Fig. 4b and c). They are composed mainly of quartz, plagioclase, K-feldspar, biotite, and muscovite. Titanite, graphite, apatite, and zircon are subordinate or small in quantity. Graphite occurs as a fine-grained flake found mostly along biotite and muscovite (Fig. 5). Carbonate, chlorite, and epidote occur as possible secondary minerals. Biotite and feldspar are mostly coarse-grained, whereas muscovite and quartz are fine-grained and occur as an aggregate. Muscovite and quartz form a layer showing microscopically schistose texture**.**

Zircon grains were separated from the samples by standard crushing and heavy-liquid techniques, and then handpicked. Zircon grains from the samples and the zircon standard QGNG with a SHRIMP ^{238}U–^{206}Pb* age of 1842.0±3.1 Ma (Black *et al.*, 2003), were mounted in an epoxy

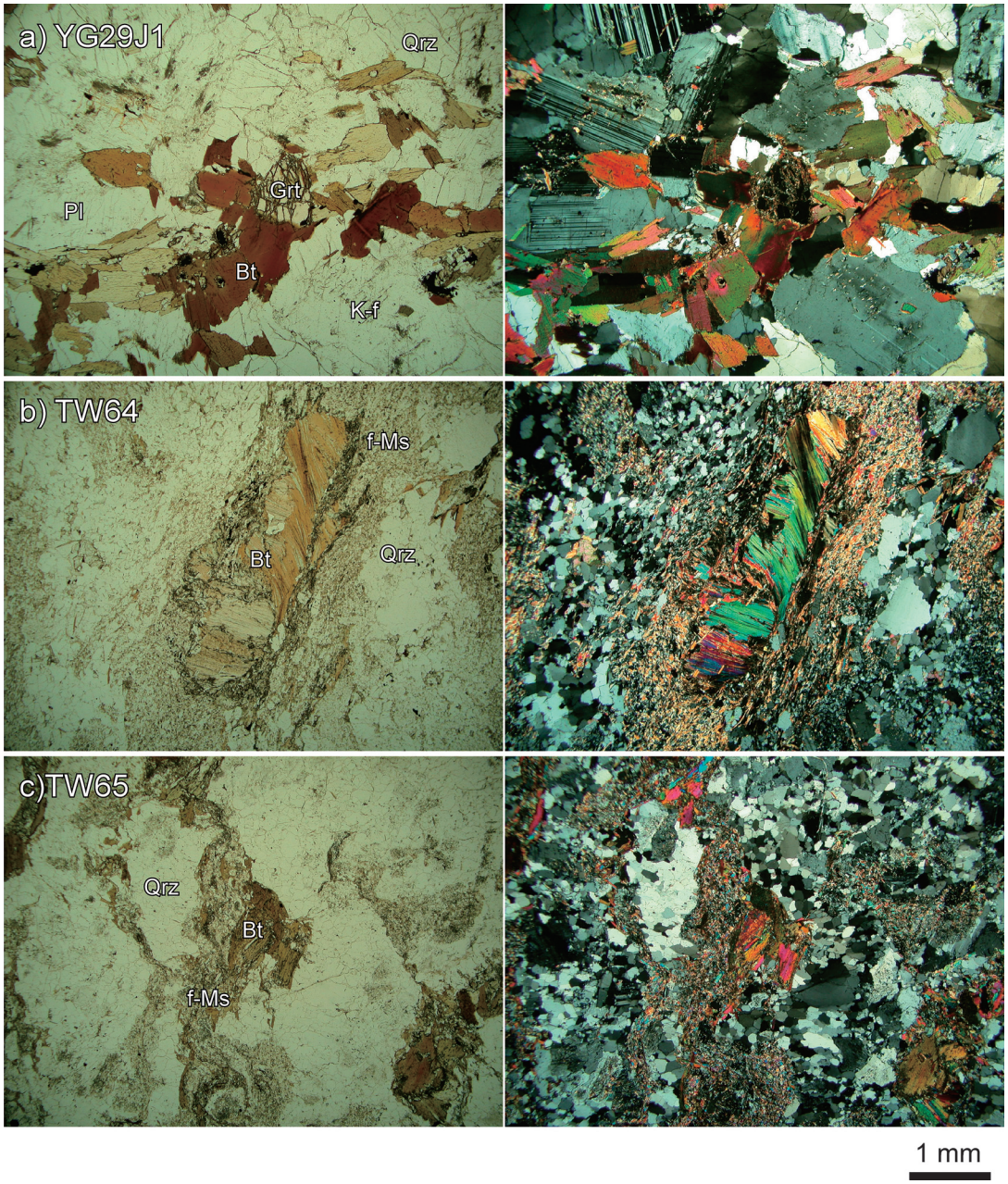

Fig. 4. Photomicrograph of the thin section of the samples; a) YG29J1, b) TW64 and c) TW65. Left and right pictures show opened and crossed polars, respectively. Qtz: quartz, Pl: plagioclase, K-f: potassium feldspar, Bt: biotite, f-Ms: fine-grained muscovite, Grt: garnet.

resin and polished until their centers were largely exposed on a flat surface. U–Pb dating was performed using a SHRIMP II system installed at Hiroshima University, Japan. Instrumental conditions and measurement procedures are described in Sano *et al.* (2000). The spot size of the primary ion beam was about 20 μm. Both backscattered images and cathodoluminescence im-

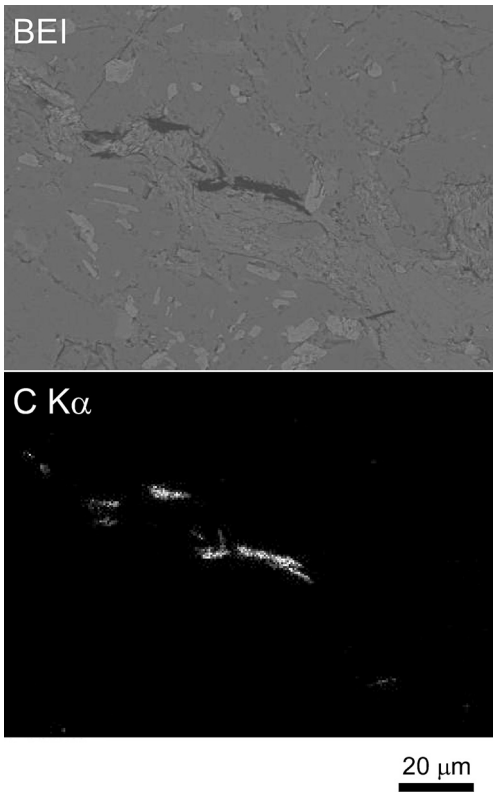

Fig. 5. Backscattered electron image (BEI) and Carbon Kα radiation image (C Kα) of graphite flake in the sample TW64.

ages were used to select sites for SHRIMP analysis. The $^{206}Pb/^{238}U$ ratios of the samples were calibrated using the empirical relationship described by Claoue-Long *et al.* (1995). In this procedure, it is essential to subtract initial Pb from measured Pb to estimate the age accurately. The measured $^{206}Pb/^{204}Pb$ ratio was used for the correction of initial Pb, whose isotopic composition was assumed using a single-stage model (Compston *et al.*, 1984).

Zircons in the orthogneiss YG29J1 were usually euhedral crystals and showed strong sector zoning under cathodoluminescence imaging (Fig. 6). They were commonly elongated crystals up to 500 microns in length. These profiles indicated rapid crystallization of the zircons (Corfu *et al.*, 2003). On the other hand, cathodoluminescence images of zircons in the samples TW64 and TW65 were characterized by distinct overgrowth. Most of the zircons have an inherited core (relatively dark part; Fig. 6) and rim (bright part; Fig. 6). Although the outer shape of the zircon was mostly euhedral, cores were anhedral to subhedral in shape and mostly showed a partly eroded texture. The sizes of the cores are up to a few hundred microns.

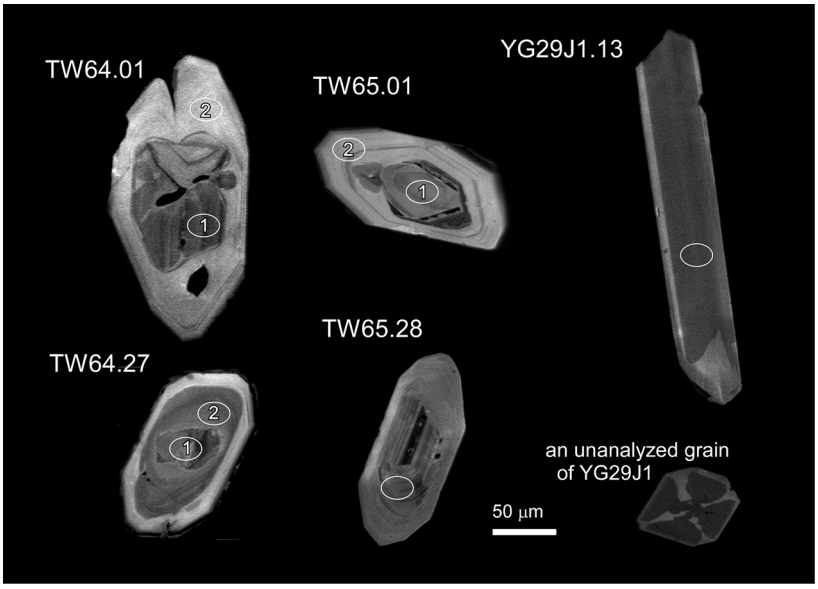

Fig. 6. Cathodoluminescence images (CL) of typical zircon grains. Ellipses on the images point to analyzed spots by SHRIMP with the sub-numbers.

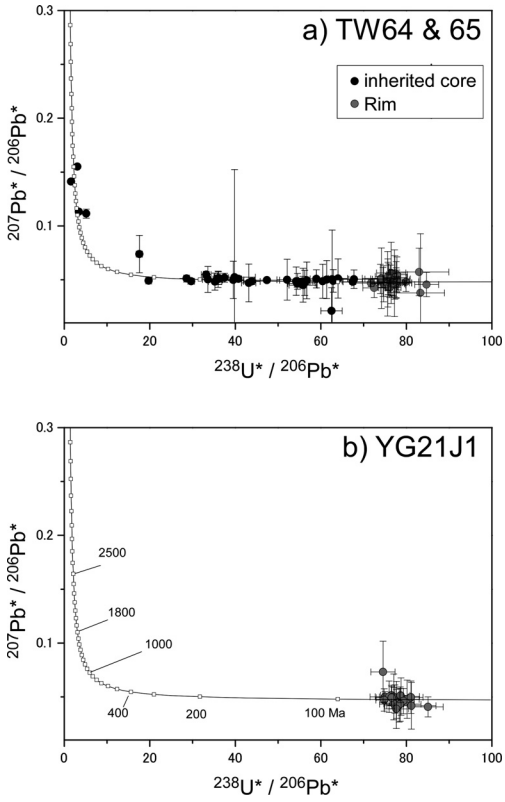

Fig. 7. Tera-Wasserberg U-Pb concordia diagram of zircons from the samples TW64 and TW65 (a) and the sample YG21J1 (b). $^{207}Pb^*$ and $^{206}Pb^*$ indicate radiometric ^{207}Pb and ^{206}Pb, respectively. Solid curve indicates concordia curve.

Results

Table 1 lists zircon data in terms of U and Th concentrations, $^{204}Pb/^{206}Pb$, $^{207}Pb/^{206}Pb$, $^{238}U/^{206}Pb$, and Th/U ratios, the radiometric $^{238}U/^{206}Pb^*$ and $^{207}Pb^*/^{206}Pb^*$ ages, and the distinction between the two analyzed areas: the core or rim. All errors are stated at 1 sigma. Sub-numbered labels such as TW64.01.1 to TW64.01.2 in the tables indicate different pit positions in a single grain.

Figure 7 shows Tera-Wasserberg concordia diagrams for all zircon data from gneiss samples. The Tera–Wasserberg concordia diagrams and $^{238}U/^{206}Pb^*$ mean ages shown in Fig. 8 were made and calculated by Isoplot 3 (Ludwig, 2003). All zircon data from orthogneiss YG29J1 plotted in a cluster and the weighted mean age is 82.2±1.3 Ma (Fig. 8a: 95% conf. tσ, MSWD=0.68). The ages of the zircon cores in paragneiss TW64 and TW65 mostly cluster between 90 to 220 Ma, except for a few data points- four grains from 1800 to 2000 Ma and two grains from 300 to 400 Ma (Fig. 7a). All zircon rim data for the samples are plotted in a cluster and the weighted mean age is 83.2±1.2 Ma (Fig 8b: 95% conf. tσ, MSWD=0.75), which is almost the same as the age of the orthogneiss mentioned above. The youngest inherited zircon core is 94.5±5.9 Ma (TW65.26.1 in Table 1).

Discussion

Protoliths and Metamorphic Age of the Gneisses in the Tailuko Belt

It is thought that the zircons in the YG29J1 sample from Yuantoushan gneiss body was formed by igneous activity of the protolith because of the internal structure and morphology of the zircon crystals. Most of the zircon grains in the sample have sector zoning which indicate rapid crystal growth, and the elongated crystal shape also indicates rapid growth of the crystals (Corfu *et al.* 2003). The zircon ages are concentrated in a cluster without any significant age variation (Fig. 6). The weighted mean age of the zircons in sample YG29J1 yield 82.2±1.3 Ma (Fig. 8a; 95% conf. tσ, MSWD=0.68). In addition to the equigranular texture of the rock and euhedral morphology of the zircons, the age data show that the age is from the protolith formation. A probable candidate for the protolith may be a granitoid or intrusive igneous rock.

On the other hand, most zircons in samples TW64 and TW65 have a core-rim structure, where a dark core and bright rim are usually observed by cathodoluminescence images (Fig. 6). Core and rim ages are commonly interpreted as protolith origin age(s) and metamorphic age, respectively. So, the weighted mean age of the rim of the zircons in samples TW64 and TW65, 83.2±1.2 Ma (Fig. 8b; 95% conf. tσ, MSWD=0.75), is considered to be the metamorphic age of

Table 1. SHRIMP U–Pb data and calculated ages of zircons.

Label	c/r	$^{204}Pb/^{206}Pb$	$^{207}Pb/^{206}Pb$	$^{238}U/^{206}Pb$	U (ppm)	Th (ppm)	Th/U	^{238}U-^{206}Pb age (Ma)	$^{207}Pb^*/^{206}Pb^*$ age (Ma)
Sample YG21J1 (orthogneiss)									
YG21J1.01.1	–	0.000281±0.001023	0.0514±0.0058	77.28±2.27	156	95	0.61	82.5±2.9	
YG21J1.02.1	–	0.000238±0.000557	0.0550±0.0029	76.17±2.40	214	142	0.66	83.7±2.8	
YG21J1.03.1	–	0.000508±0.000784	0.0555±0.0041	76.57±2.92	186	122	0.65	82.9±3.4	
YG21J1.04.1	–	0.000803±0.000959	0.0543±0.0027	77.14±3.04	220	95	0.43	81.8±3.5	
YG21J1.05.1	–	0.000135±0.000273	0.0519±0.0021	74.82±3.45	322	249	0.77	85.4±3.9	
YG21J1.06.1	–	0.001665±0.001010	0.0748±0.0039	76.32±3.93	310	238	0.77	81.3±4.4	
YG21J1.07.1	–	−0.001408±0.001908	0.0531±0.0022	76.48±1.20	341	176	0.52	85.9±3.2	
YG21J1.08.1	–	0.000778±0.001084	0.0593±0.0034	79.03±2.26	159	67	0.42	79.9±2.8	
YG21J1.09.1	–	0.000599±0.001308	0.0588±0.0035	76.21±2.77	132	52	0.39	83.1±3.6	
YG21J1.10.1	–	0.000982±0.000865	0.0583±0.0053	75.66±1.95	145	61	0.42	83.1±2.5	
YG21J1.11.1	–	0.000662±0.000883	0.0599±0.0034	75.06±2.98	207	123	0.60	84.3±3.6	
YG21J1.12.1	–	0.000251±0.000395	0.0550±0.0021	78.29±2.09	457	389	0.85	81.4±2.2	
YG21J1.13.1	–	0.000528±0.000615	0.0571±0.0033	75.85±3.50	165	71	0.43	83.6±4.0	
YG21J1.14.1	–	0.000671±0.000565	0.0507±0.0021	84.01±3.40	535	281	0.53	75.3±3.1	
YG21J1.15.1	–	0.000486±0.000922	0.0569±0.0032	80.34±2.42	283	214	0.76	79.0±2.7	
YG21J1.16.1	–	0.000629±0.000722	0.0554±0.0020	78.40±2.26	356	115	0.32	80.8±2.6	
YG21J1.17.1	–	0.000870±0.000965	0.0561±0.0034	77.30±4.54	200	124	0.62	81.5±5.0	
YG21J1.18.1	–	0.000616±0.001338	0.0509±0.0032	80.25±5.34	132	54	0.41	78.9±5.6	
YG21J1.19.1	–	0.001063±0.001099	0.0546±0.0030	76.13±2.26	152	67	0.44	82.5±3.0	
YG21J1.20.1	–	0.000365±0.000633	0.0525±0.0026	74.32±1.74	224	145	0.64	85.6±2.2	
Sample TW64 (paragneiss)									
TW64.01.1	c	0.000743±0.001067	0.0607±0.0020	38.97±2.34	213	203	0.96	161.1±10.1	
TW64.01.2	r	0.001004±0.001720	0.0662±0.0027	72.78±3.70	258	51	0.20	86.3±5.2	
TW64.02.1	c	0.000014±0.000024	0.0511±0.0011	40.72±0.76	2213	1806	0.82	156.4±2.9	
TW64.02.2	r	0.000880±0.001009	0.0677±0.0026	76.54±1.95	238	58	0.24	82.3±2.6	
TW64.03.1	c	0.000531±0.000437	0.0564±0.0018	54.01±1.85	413	282	0.68	117.1±4.1	
TW64.04.1	c	0.001081±0.000456	0.0664±0.0013	35.27±0.56	491	187	0.38	176.7±3.1	
TW64.05.1	r	0.001459±0.001862	0.0684±0.0027	75.13±2.85	238	115	0.48	82.9±4.3	
TW64.06.1	c	0.001732±0.002730	0.0759±0.0030	60.65±2.04	175	373	2.14	102.1±6.3	
TW64.07.1	c	0.000310±0.000359	0.0561±0.0014	35.87±0.93	418	152	0.36	176.3±4.7	
TW64.08.1	r	0.000716±0.000403	0.0536±0.0015	74.72±2.32	747	357	0.48	84.6±2.7	
TW64.10.1	r	0.001321±0.001707	0.0757±0.0036	74.58±2.28	213	75	0.35	83.8±3.7	
TW64.09.1	c	0.000995±0.001106	0.0658±0.0030	62.85±1.71	156	178	1.15	99.9±3.4	
TW64.09.2	r	0.001351±0.001017	0.0696±0.0028	75.69±2.59	256	88	0.34	82.5±3.2	
TW64.11.1	c	0.001374±0.000924	0.0688±0.0039	58.89±1.98	174	166	0.95	105.8±4.0	
TW64.12.1	r	0.000931±0.000529	0.0562±0.0022	71.20±2.46	664	1293	1.95	88.4±3.2	
TW64.15.1	c	0.004979±0.005201	0.1254±0.0102	36.18±2.12	29	24	0.82	159.8±19.1	
TW64.16.1	c	0.001268±0.001135	0.0687±0.0032	50.91±2.06	229	88	0.38	122.5±5.6	
TW64.16.2	r	0.003425±0.003044	0.0890±0.0059	77.99±2.37	142	58	0.41	76.9±5.2	
TW64.17.1	c	0.000022±0.000008	0.1414±0.0011	1.59±0.08	2077	251	0.12	3152±118	2241±13
TW64.19.1	c	0.001152±0.000787	0.0656±0.0026	53.09±1.68	232	183	0.79	117.8±4.1	
TW64.19.2	r	0.000922±0.000678	0.0592±0.0022	83.29±2.52	527	76	0.14	75.6±2.5	
TW64.20.1	c	0.001137±0.001020	0.0662±0.0035	55.50±1.50	155	82	0.53	112.7±3.7	
TW64.21.1	c	0.001152±0.001058	0.0671±0.0032	60.09±1.69	183	153	0.84	104.2±3.6	
TW64.22.1	c	0.000036±0.000093	0.0521±0.0013	36.09±0.70	568	263	0.46	176.1±3.4	
TW64.23.1	r	0.001022±0.000815	0.0631±0.0023	73.15±2.07	341	151	0.44	85.9±2.8	
TW64.27.1	c	0.000009±0.000009	0.1552±0.0009	3.08±0.16	1603	1150	0.72	1812±84	2403±10
TW64.27.2	c	0.000059±0.000026	0.1122±0.0041	5.13±0.12	830	15	0.02	1147±25	1822±66
TW64.33.1	c	0.000176±0.000113	0.0513±0.0011	29.58±0.73	1300	665	0.51	213.6±5.2	
TW64.34.1	c	0.000260±0.000151	0.0530±0.0017	19.63±0.31	431	276	0.64	318.8±5.0	
Sample TW65 (paragneiss)									
TW65.01.1	r	0.000442±0.000549	0.0546±0.0024	79.24±2.87	319	66	0.21	80.2±3.0	
TW65.01.2	c	0.000002±0.000006	0.1133±0.0013	3.40±0.10	1010	121	0.12	1661±43	1852±20
TW65.02.1	r	0.000771±0.000908	0.0611±0.0032	74.81±2.37	161	23	0.14	84.4±3.0	

$^{206}Pb^*$ and ^{207} Pb* mean radiometric ^{206}Pb and ^{207}Pb, respectively.
The c/r column indicates attributiion of the analyzed points, core(c) or rim(r).

Table 1. (Continued)

Label	c/r	$^{204}Pb/^{206}Pb$	$^{207}Pb/^{206}Pb$	$^{238}U/^{206}Pb$	U (ppm)	Th (ppm)	Th/U	^{238}U-^{206}Pb age (Ma)	$^{207}Pb^*/^{206}Pb^*$ age (Ma)
TW65.02.2	c	0.000275±0.000247	0.0560±0.0014	37.32±0.89	340	298	0.88	169.6±4.1	
TW65.03.1	r	0.000287±0.001258	0.0563±0.0033	76.90±2.12	231	64	0.28	82.8±3.0	
TW65.03.2	r	0.000417±0.000346	0.0524±0.0018	77.34±1.91	479	72	0.15	82.2±2.1	
TW65.04.1	r	0.000586±0.000661	0.0539±0.0026	76.35±2.40	215	31	0.15	83.0±2.8	
TW65.04.2	c	0.000343±0.000172	0.0517±0.0021	54.11±2.18	984	2568	2.61	117.3±4.7	
TW64.05.1	r	0.000971±0.000993	0.0607±0.0044	73.33±2.72	202	52	0.26	85.8±3.5	
TW65.05.2	c	0.001416±0.000934	0.0659±0.0028	54.38±3.05	186	88	0.47	114.4±6.7	
TW65.06.1	r	0.000709±0.000821	0.0612±0.0034	72.96±3.40	157	67	0.43	86.6±4.2	
TW65.07.1	r	0.000771±0.000672	0.0586±0.0038	75.27±2.55	161	41	0.26	83.9±3.0	
TW65.08.1	r	0.000522±0.000755	0.0585±0.0039	75.53±4.47	141	55	0.39	84.0±5.1	
TW65.08.2	c	0.000022±0.000044	0.0500±0.0013	47.37±2.94	4359	1128	0.26	134.6±8.3	
TW65.09.1	r	0.000128±0.000189	0.0488±0.0016	71.58±4.49	685	36	0.05	89.2±5.6	
TW65.09.2	c	0.000440±0.000728	0.0568±0.0029	33.30±1.14	96	38	0.40	189.2±6.8	
TW65.10.1	r	0.000770±0.000552	0.0541±0.0023	75.03±2.45	443	362	0.82	84.1±2.9	
TW65.11.1	r	0.001228±0.001323	0.0752±0.0039	81.08±6.47	302	79	0.26	77.2±6.4	
TW65.11.2	c	0.000079±0.000145	0.0497±0.0020	43.79±1.96	828	352	0.42	145.4±6.4	
TW65.12.1	r	0.000253±0.000462	0.0520±0.0030	75.27±2.14	255	79	0.31	84.7±2.5	
TW65.13.1	r	0.000804±0.000839	0.0591±0.0028	76.46±2.77	221	43	0.20	82.5±3.2	
TW65.15.1	r	0.000528±0.000807	0.0609±0.0029	74.96±2.71	239	43	0.18	84.6±3.3	
TW65.15.2	c	0.000069±0.000147	0.0522±0.0023	28.57±0.87	357	297	0.83	221.5±6.7	
TW65.17.1	r	0.000328±0.000604	0.0538±0.0024	77.28±2.16	279	45	0.16	82.4±2.5	
TW65.17.2	r	0.001349±0.001336	0.0670±0.0035	73.79±3.37	173	82	0.47	84.6±4.4	
TW65.18.1	c	−0.000633±0.001110	0.0648±0.0036	17.77±0.63	51	22	0.44	356±14	1038±413
TW65.20.1	r	0.000633±0.000721	0.0566±0.0031	75.96±4.19	261	74	0.28	83.3±4.7	
TW65.20.2	c	0.002349±0.001244	0.0569±0.0032	59.78±1.90	228	170	0.75	102.3±4.1	
TW65.20.3	c	0.000361±0.000646	0.0544±0.0022	62.47±1.93	278	334	1.20	101.7±3.3	
TW65.21.1	c	0.000308±0.000718	0.0516±0.0026	55.93±2.29	244	209	0.85	113.6±4.9	
TW65.22.1	r	0.000940±0.001838	0.0601±0.0033	74.30±2.85	173	71	0.41	84.7±4.4	
TW65.22.2	c	0.000620±0.000510	0.0600±0.0021	58.30±1.37	333	232	0.70	108.4±2.7	
TW65.23.1	c	0.000016±0.000044	0.0486±0.0020	55.61±1.49	593	485	0.82	114.9±3.1	
TW65.25.1	c	0.000060±0.000105	0.0557±0.0026	33.16±1.14	173	63	0.37	191.4±6.5	
TW65.25.2	c	0.000254±0.000308	0.0545±0.0018	35.68±1.01	268	106	0.40	177.4±5.0	
TW65.24.1	c	0.000068±0.000133	0.0491±0.0012	67.41±2.27	1346	22	0.02	94.8±3.2	
TW65.26.1	c	0.000250±0.000514	0.0541±0.0028	67.42±4.23	165	93	0.57	94.5±5.9	
TW65.27.1	c	0.001365±0.001050	0.0673±0.0026	42.06±1.40	144	92	0.64	147.7±5.7	
TW65.28.1	c	0.000315±0.000326	0.0524±0.0018	55.50±1.60	435	403	0.93	114.5±3.3	
TW65.29.1	c	0.000305±0.000477	0.0528±0.0023	35.05±1.54	141	66	0.47	180.3±8.0	

$^{206}Pb^*$ and ^{207} Pb* mean radiometric ^{206}Pb and ^{207}Pb, respectively.
The c/r column indicates attributiion of the analyzed points, core(c) or rim(r).

the paragneisses. Metamorphic zircons yield a low Th/U ratio (ca. <0.1: Hoskin and Black, 2000). The Th/U ratios of the rims are mostly lower than the zircons in orthogneiss sample YG29J1 (Fig. 9). Although the Th/U ratio of the rim data is higher than 0.1, the lithology of the sample, inner structures, and ages of the zircon grains show that the rims were newly formed around detrital zircon grains by metamorphism which formed the paragneiss. Hence, 'Th/U= 0.1' is not an absolute criterion used to interpret igneous or metamorphic origins. The age of the zircon rims from the paragneiss is essentially the same as that of zircon in the orthogneiss.

The previous age data of granitoids in the Eastern Central Range range from 77 to 97 Ma (Lan *et al.*, 1996). The age of zircons in sample YG29J1 and the rim of TW64 and TW65, are not only consistent with previous data but are of relatively high precision. However, new SHRIMP data by Yui *et al.* (2009) indicate slightly older ages; 87–88 Ma. Their MSWD values are around

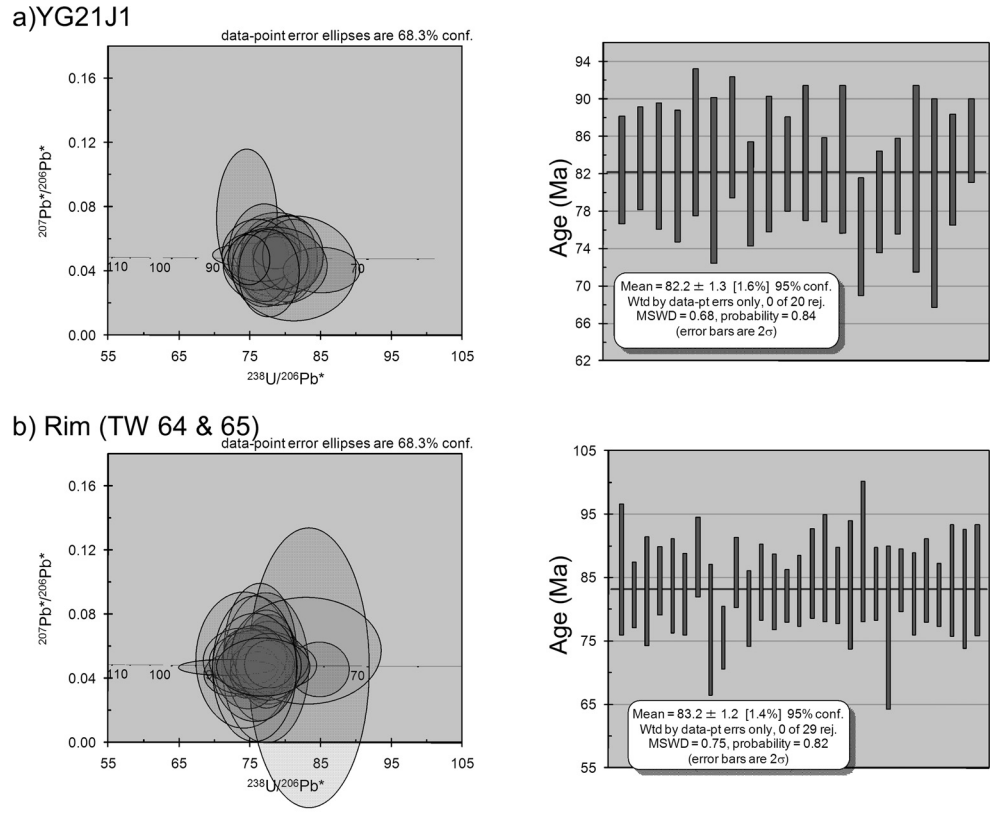

Fig. 8. Tera-Wasserberg U–Pb concordia diagrams of zircons and ^{238}U–^{206}Pb age distribution plot of the rim data of the samples TW64 and TW65 (a) and all data of the sample YG21J1 (b). $^{207}Pb^*$ and $^{206}Pb^*$ indicate radiometric ^{207}Pb and ^{206}Pb, respectively. Solid curve indicates concordia curve.

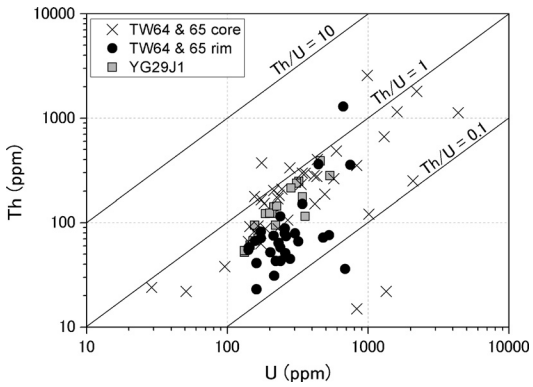

Fig. 9. U-Th relations of all analyzed spots. The lines indicate Th/U ratios for reference.

3, which is far higher than the MSWD around 0.7 for the present results. As the MSWD value is one of the most important criteria for the reliability of mean ages, the difference of the ages between the two SHRIMP machines may be due to the different MSWD values. In addition to the standard selections, different localities may be one of the major reasons for the minor difference of the two age results.

Origin of Zircon Core in the Paragneiss Samples (TW64 and TW65)

Most of the zircons in the paragneiss samples have overgrowth rims which formed by metamorphism at 83.2±1.2 Ma. The age is essentially the same as that of the previously mentioned orthogneiss. It may suggest that the protolith of the orthogneiss was a synkinematic intrusion or a pluton. On the other hand, the cores of zircons have various ages ranging from the Paleoprotero-

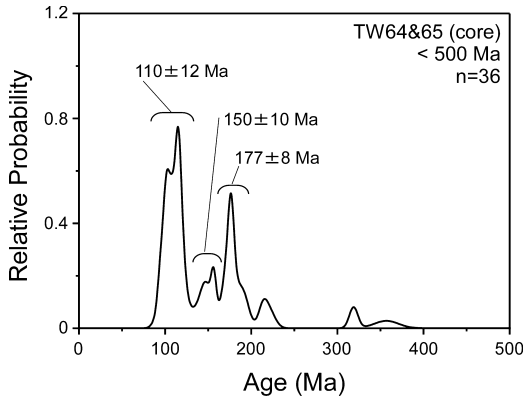

Fig. 10. Probability distribution diagrams of zircon core ages from samples integration TW64 and TW65.

zoic to Late Cretaceous. In addition to the presence of graphite in the gneiss, the age variation, subhedral nature, and the corroded texture of the zircon core indicate that the zircon core was detrital and the protolith of the paragneiss was relatively coarse-grained sediment. The youngest age of the zircon core was 94.5±5.9 Ma, which is thought to be the older limit on deposition age of the protolith while the younger limit is the metamorphism age (*e.g.* Tsutsumi *et al.*, 2009). So, deposition age of the protolith must be between 95 Ma and 83 Ma and the protolith is considered to be Late Cretaceous sedimentary rock. Generally, age distribution of zircons is useful to estimate the provenance of sedimentary materials. The zircon age distribution of the paragneisses has some younger peaks (ca. 110, 150, 180 Ma; Fig. 10), and they are consistent with Yanshanian magmatism, SE China (*e.g.* Jahn *et al.*, 1986). Some zircons have ages from 1800 to 2000 Ma. Such old zircon is not uncommon in SE China (Xu *et al.*, 2007). Thus paragneisses in the northern Tailuko Belt originate from the clastics of SE China deposited after 95 Ma and metamorphosed in 83 Ma.

The Tailuko Belt consists mainly of pelitic schist, gneiss, migmatite, metamorphosed limestone, greenschist, siliceous schist, and amphibolite. The age of the belt is based on the age of various components within the belt and includes 250±20 Ma (Sr isotopic stratigraphy; Jahn *et al.*, 1984) for marble, Permina Fusulinids assemblage in the marble (Lee, 1984), and a Mesozoic dinoflagellate fossil *Eyachia* (?) in metapelite (175–200 Ma; Chen, 1989). Some of these data conflict with the present results from the zircons in the gneiss. The Tailuko belt apparently includes a member of the subduction complex-limestone (or marble), chert (or siliceous schist), basaltic rocks (or greenschist and amphibolite), and pelagic mudstone (or metapelite?). The conflict may be explained by a scenario that the pre-Cretaceous rocks were exotic blocks brought by the oceanic plate into the subduction zone during the Late Cretaceous.

Conclusion

1. The weighted mean age of zircons of the orthogneiss YG29J1 sample from the Yuantoushan gneiss body yields 82.2±1.3 Ma (Fig. 8a; 95% conf. tσ, MSWD=0.68) which is considered to be formed by igneous activity of the protolith.
2. The zircons in the paragneiss samples TW64 and TW65 from the Takkili gneiss body have metamorphic rims. The weighted mean age of the zircon rims, 83.2±1.2 Ma (Fig. 8b; 95% conf. tσ, MSWD=0.75), is considered to be the metamorphic age of the paragneisses.
3. The protoliths of the paragneisses (TW64 and TW65) are Late Cretaceous sedimentary rocks because the youngest age of detrital zircon cores yields 94.5±5.9 Ma which is considered to be the older limit on deposition age.
4. The younger age distribution of the zircon core is similar to the Yanshanian magmatism (ca. 110, 150, 180 Ma) in SE China where it is a probable candidate for the provenance of the detrital zircons in paragneiss.

Acknowledgements

We wish to express our sincere thanks to Mrs. M. Shigeoka of the National Science Museum for her help in sample preparations and SEM

analysis. We also grateful to Dr. S. Suto of the National Institute of Advanced Industrial Science and Technology (AIST) for helpful comments. This is a contribution from the Hiroshima SHRIMP Laboratory.

References

Black, L. P., Kamo, S. L., Williams, I. S., Mundil, R., Davis, D. W., Korsch, R. J. and Foudoulis, C. (2003) The application of SHRIMP to Phanerozoic geochronology; a critical appraisal of four zircon standards. *Chemical Geology*, **200**: 171–188.

Chen, C. H. (1989) A preliminary study of the fossil dinoflagellates from the Tananao Schist, Taiwan: Master Thesis, NTU, Taiwan, 89 pp. (in Chinese)

Chen, P. Y. (1963) Mineralogy and petrology of the chloritoid rock from Shakatangchi and Laohsichi, Hualien, Taiwan. *Acta Geologica Taiwanica*, **13**: 9–20.

Cherniak, D. J. and Watson, E. B. (2000) Pb diffusion in zircon. *Chemical Geology* **172**: 5–24.

Claoue-Long, J. C., Compston, W., Roberts, J. and Fanning, C. M. (1995) Two Carboniferous ages: a comparison of SHRIMP zircon dating with conventional zircon ages and $^{40}Ar/^{39}Ar$ analysis. In Berggren, A., Kent D. V., Aubly, M.-P., Hardenbol, J. (Ed.), *Geochronology, Time Scales and Global Stratigraphic Correlation*. Society for sedimentary Geology Special Publication, 54, Society for Sedimentary Geology Tulsa, pp 3–21.

Compston, W., Williams, I.S. and Meyer, C. (1984) U–Pb geochronology of zircons from lunar breccia 73217 using a sensitive high mass-resolution ion microprobe. *Journal of Geophysical Research* **89**: Supplement, B525–534.

Corfu, F., Hancher, J. M., Hoskin, P. W. O. and Kinny, P. (2003) An atlas of zircon textures. In Hancheer, J. M. and Hoskin, P. W. O (Ed.), *Zircon: Reviews in Mineralogy and Geochemistry 53*, pp. 278–286. Mineralogical Society of America, Washington D.C.

Hoskin, P. W. and Black, L. P. (2000) Metamorphic zircon formation by solid-state recrystallization of protolith igneous zircon. *Journal of Metamorphic Geology*, **18**: 423–439.

Ho, C. S. (1986a) A synthesis of the geologic evolution of Taiwan. *Tectonophysics*, **125**: 1–16.

Ho, C. S. (1986b) An introduction to the geology of Taiwan. 192 pp. Central Geological Survey, the Ministry of Economic Affairs, Taiwan, Republic of China.

Jahn, B. M., Chi, W. R. and Yui, T. F. (1992) A Late Permian formation of Taiwan (marbles from Chia-Li well No. 1): Pb-Pb isochron and Sr isotopic evidence, and its regional geological significance. *Journal of the Geological Society of China*, **35**: 193–218.

Jahn, B. M., Martineau, F., Peucat, J. J., and Cornichet, J. (1986) Geochronology of the Tananao Schist Complex, Taiwan, and its regional tectonic significance. *Tectonophysics*, **125**: 103–124.

Jahn, B. M., Martineau, F. and Cornichet, J. (1984) Chronological significance of Sr isotopic compositions in the crystalline limestones of the Central Range, Taiwan. *Memoirs of the Geological Society of China*, **7**: 383–404.

Lan, C. Y., Chen, C. H., Chen, C. H., Chung, S. L., Lee, T., Wang Lee, C. M. and Yui, T. F. (1996) The crustal evolution of continental Taiwan. *Journal of the Geological Society of China*, **39**: 337–353.

Lee, C. S. (1984) Stratigraphic study of the Tananao Group in the region north of Liwuchi, Taiwan. *Special Publication of the Central Geological Survey*, **3**: 1–10 (in Chinese with English abstract).

Lee, J. K., Wiliams, I. and Ellis, D. J. (1997) Pb, U and Th diffusion in natural zircon. *Nature*, **390**: 159–162.

Ludwig, K. R. (2003) User's manual for Isoplot 3.00. A geochronological toolkit for Microsoft Excel. Berkeley Geochronology Center Special Publication No. 4, pp. 70, Berkeley Geochronology Center, Berkeley, CA., USA.

Sano, Y., Hidaka, H., Terada, K., Shimizu, H. and Suzuki, M. (2000) Ion microprobe U–Pb zircon geochronology of the Hida gneiss: Finding of the oldest minerals in Japan. *Geochemical Journal*, **34**: 135–153.

Sano, Y., Terada, K., Hidaka, H., Yokoyama, K. and Nutman, A. P. (1999) Palaeoproterozoic thermal events recorded in the ~4.0 Ga Acasta gneiss, Canada: Evidence from SHRIMP U–Pb dating of apatite and zircon. *Geochimica et Cosmochimica Acta*, **63**: 899–905.

Tsutsumi, Y., Miyashita, A., Terada, T. and Hidaka, H. (2009) SHRIMP U–Pb dating of detrital zircons from the Sanbagawa Metamorphic Belt, Kanto Mountains, Japan: need to revise the framework of the belt. *Journal of Mineralogical and Petrological Sciences*, **104**: 12–24.

Yen, T. P. (1954) The gneisses of Taiwan. *Bulletin of the Geological Survey of Taiwan*, **5**: 1–99.

Yen, T. P. and Yeh, Y.-H. (1990) Geotransects in the Taiwan Region. *EOS*, American Geophysical Union, **71**: 353.

Yui, T. F., Okamoto, K., Usuki, T., Lan, C. Y., Chu, H. T. and Liou, J. G. (2009) Late Triassic – Late Cretaceous accretionary/subduction in the Taiwan region along the eastern margin of South China—evidence from zircon SHRIMP dating. *International Geology Review*, **51**: 304–328.

Xu, X., O'Reilly, S. Y., Griffin, W. L., Wang, X., Pearson, N.J. and He, Z. (2007) The crust of Cathaysia: Age, assembly and reworking of two terrane. *Precambrian Research*, **158**: 51–78.